Induced earthquakes in the development of unconventional energy resources

YANG HongFeng[1], LIU YaJing[2], WEI Meng[3], ZHUANG JianCang[4] & ZHOU ShiYong[5]

[1] *Earth System Science Programme, Faculty of Science, Chinese University of Hong Kong, Hong Kong 999077, China;*
[2] *Earth and Planetary Sciences, McGill University, Montréal, Québec H3A 2A7, Canada;*
[3] *Graduate School of Oceanography, University of Rhode Island, Narragansett, Rhode Island 02882, USA;*
[4] *Institute of Statistical Mathematics, Tokyo 190-8562, Japan;*
[5] *ITAG Institute of Theoretical and Applied Geophysics, Peking University, Beijing 100871, China*

Abstract   It has long been known that human activities such as waste fluid disposal and reservoir impoundment may cause earthquakes. Recently, anthropogenic activities to tackle the increasing energy demand and to address climate change issues are also reported to induce earthquakes. These activities have a common attribute in that fluids are injected and extracted underground and induce spatiotemporal changes of pore pressure and stress, which may cause slip on faults. Induced earthquakes not only pose significant impacts on seismic hazard assessment and preparation, but also raise the question to the society as how to balance the economic needs of resources development and the public's concerns about potential environmental impacts. Here we review the observations of fluid-injection/extraction induced earthquakes, ground deformation associated with these activities, and their physical mechanisms. Furthermore, we discuss the influences of induced earthquakes on seismic hazard models, regulatory policies on these anthropogenic activities, and current development of academic, industrial and government initiatives and collaborations in order to understand this intriguing phenomenon and address associated challenges.

Keywords   Induced earthquake, Fluid injection, Energy demand, Climate change

1.   Introduction

Earthquakes are a major threat to the human society, as vividly demonstrated by the recent 2011 M_w9.0 Tohoku-oki (Japan), 2015 M_w8.3 Illapel (Chile), and 2015 M_w7.8 Gorkha (Nepal) earthquakes (e.g., Yue and Lay, 2011; Yang et al., 2015; Yin et al., 2016, 2017). Accordingly a major challenge in hazard mitigation is the fundamental understanding of earthquake physics, so that appropriate societal responses can be formulated for mitigating major seismic risk to human lives and infrastructure. In addition to tectonic earthquakes, it has long been known that human activities such as water

reservoir impoundment and waste fluid disposal may cause earthquakes, termed induced earthquakes (e.g. McGarr et al., 2002). Consequently there have been relevant review papers to discuss this intriguing phenomenon, mostly focusing on the overview of case studies of well documented induced earthquakes. For instance, Nicholson and Wesson (1992) summarized the earthquakes triggered by deep well activities, including deep well fluid injection and massive fluid extraction. Talwani (1997) documented reservoir-induced earthquakes and discussed two categories of seismicity by their occurrence time relative to the initial impoundment. McGarr et al. (2002) reviewed case histories of anthropogenic seismicity, including mining, quarry, fluid injection, large impounded reservoirs, as well as hydrocarbon reservoir

---

* Corresponding author (email: hyang@cuhk.edu.hk)

compaction.

In recent decades, there is also heightened concern of a further complication, in that anthropogenic activities tackling climate change and energy demand (e.g. hydraulic fracturing for shale gas exploration, large-volume wastewater disposal, natural gas storage and extraction cycles) can induce seismicity and trigger relatively large quakes. After assembling 70 cases of hydrocarbon fields for which a connection between unusual seismicity patterns and hydrocarbon production had been suggested, Suckale (2009) found a striking feature that occurrences of induced earthquakes had a distinct regional character. Ellsworth (2013) reviewed the increase in seismic activity that may be primarily related with fluid injection into deep wells to dispose wastewater partly produced in hydraulic fracturing in central and eastern United States. Mostly recently, Grigoli et al. (2017) presented a summary of observations and outstanding questions in the monitoring, discrimination and management of earthquakes induced by various anthropogenic sources in Europe.

Even though there is a clear link between induced earthquakes and anthropogenic activities, many critical questions regarding this intriguing phenomenon remain unanswered. Consequently controversy has emerged regarding whether certain cases of seismicity had been indeed triggered by human activities. For instance, in Barnett Shale and Cogdell, Texas, the question was raised whether extensive development of unconventional gas resources has resulted in injection-induced earthquakes (Frohlich, 2012; Gan and Frohlich, 2013). In this paper, we do not attempt to provide an exhaustive review of all types of induced earthquakes. Rather of being region specific as in several recently published review articles, we categorize the induced seismicity observations by their potential triggering sources and focus the discussion on their physical mechanisms, hazard and regulatory policy implications. In addition to seismological observations, which constitutes the bulk of data available up to date for induced earthquakes, we also discuss other types of observations (e.g., geodetic surveys) and approaches (e.g., statistics analysis, numerical modeling) that can contribute to our understanding of the source processes. We acknowledge that the study of induced earthquakes is evolving so rapidly that some parts of this review may soon be outdated. Nevertheless, given the dramatic increase in numbers of earthquakes related to unconventional energy resources exploration in the past decade, this article aims to serve as a timely introduction to current issues in induced seismicity of interest to seismologists and the general public.

2. Seismic and geodetic observations

In view of the long history of induced seismicity documented in previous reviews (e.g. Nicholson and Wesson, 1992; McGarr et al., 2002; Ellsworth, 2013), this article focuses on

more recent anthropogenic activities to tackle energy demand and climate change, specifically, earthquakes potentially induced by (1) hydraulic fracturing (fracking), (2) waste water disposal, (3) geothermal energy extraction, (4) CO_2 sequestration, and (5) cyclic injection/extraction of natural gas (Figure 1). In this section, we introduce seismological and geodetic observations of earthquake activity and ground deformation associated with the above five scenarios.

2.1 Observed induced seismicity

It is well known that induced seismicity can be caused by the injection of waste fluid into disposal wells. A textbook example is the series of large earthquakes in the Denver area in the 1960s, due to hazardous waste injection at Rocky Mountain Arsenal in Colorado (Evans, 1966; Healy et al., 1968). In the 1970s an interdisciplinary study was undertaken in this site, synthesizing comprehensive investigations in seismology, hydrogeology and rock physics. This integrated effort has contributed to seminal advances in our understanding of the mechanics of induced seismicity (Raleigh et al., 1976). More recently, significant seismicity likely related to the disposal of wastewater in wells has been widely observed, especially in large areas long considered to be geologically stable (e.g. Petersen et al., 2016). Some of the earthquakes caused by the disposal of fluids are relatively strong and widely felt at large distances. For instance, two moderate-sized earthquakes (M_w5.7 in 2011 and M_w5.8 in 2016) in Oklahoma likely related to large volume wastewater disposal in nearby wells were felt in at least 17 states and caused damage in the epicentral region (Keranen et al., 2014; McGarr et al., 2015; Yeck et al., 2017).

Compared to wastewater disposal, hydraulic fracturing (fracking), an innovative technique to stimulate fracture growth and increase permeability so as to extract gas from the low-permeability shale formation, had been thought to induce typically small earthquakes with magnitude less than M_w1. However, a few recent cases have shown that magnitudes of earthquakes related to fracking may exceed M_w4 (British Colombia Oil and Gas Commission, 2012; Ellsworth, 2013; Atkinson et al., 2016). As shown in Figure 2, Fox Creek in Alberta, Canada, used to be a seismically quiescent area before the hydraulic fracturing operation started in March 2010. Seismicity has dramatically increased since December 2013 when fracking induced earthquakes were first reported in this area (Schultz et al., 2017).

Earthquakes have also been reported to associate with the exploitation of geothermal resources, in which water is pumped into and out of a reservoir (e.g. Häring et al., 2008; Goertz-Allmann et al., 2011; Brodsky and Lajoie, 2013). In the Salton Sea Geothermal Field, USA, long-term evolution of seismicity appears to be modulated by the net fluid volume (the difference between extraction and injection) (Brodsky

and Lajoie, 2013). Extensive microseismicity was detected during the fracturing process at the European Geothermal Hot Dry Rock research site at Soultz-sous-Forêts, France, where hydraulic stimulation is applied to enhance reservoir permeability and heat exchange efficiency. The largest events of $M_L 2.7$ to $M_L 2.9$ occurred during the shut-in period (Michelet and Toksöz, 2007). The Enhanced Geothermal System (EGS) project in Basel, Switzerland, is arguably the most notable example of earthquakes directly related to hydraulic stimulation in the process of exploiting geothermal resources. Earthquakes of $M_L 2.6$ and $M_L 3.4$ were induced during the peak injection and after well shut-in, respectively, which caused damages to local residences (Giardini, 2009). Public concern over induced seismicity eventually led to the definitive suspension of the Basel EGS project.

The fourth scenario is in connection with underground storage of natural gas, adopted worldwide to meet seasonal variations in demand, which requires cyclic injection and extraction of natural gas underground (e.g. Priolo et al., 2015). For instance, near the Hutubi gas reservoir in Xinjiang, the largest underground repository for natural gas in China, a sequence of earthquakes occurred soon after the injection was initiated in 2013, with the largest magnitude of $M_L 3.5$ (Figure 3).

The fifth scenario is to capture and sequestration of CO_2 in deep geological formations, proposed as an option to mitigate global warming due to anthropogenic emission of greenhouse gases. It has been suggested that this could result in reduction in CO_2 emissions over the century that is comparable to that expected from efficiency improvements and large-scale deployment of renewable energy resources (IPCC, 2005). How-
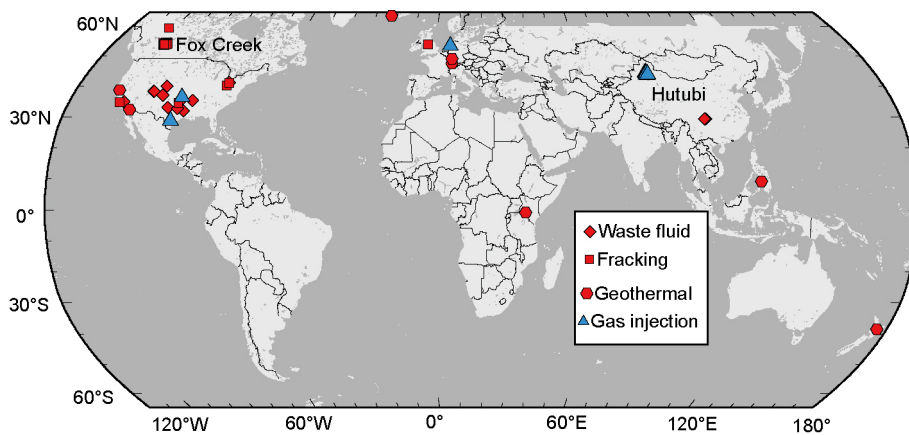
Figure 1   A global map showing reported induced earthquakes. Fox Creek, Alberta, Canada and Hutubi, Xinjiang, China are marked where local seismicity is shown in Figures 2 and 3, respectively.
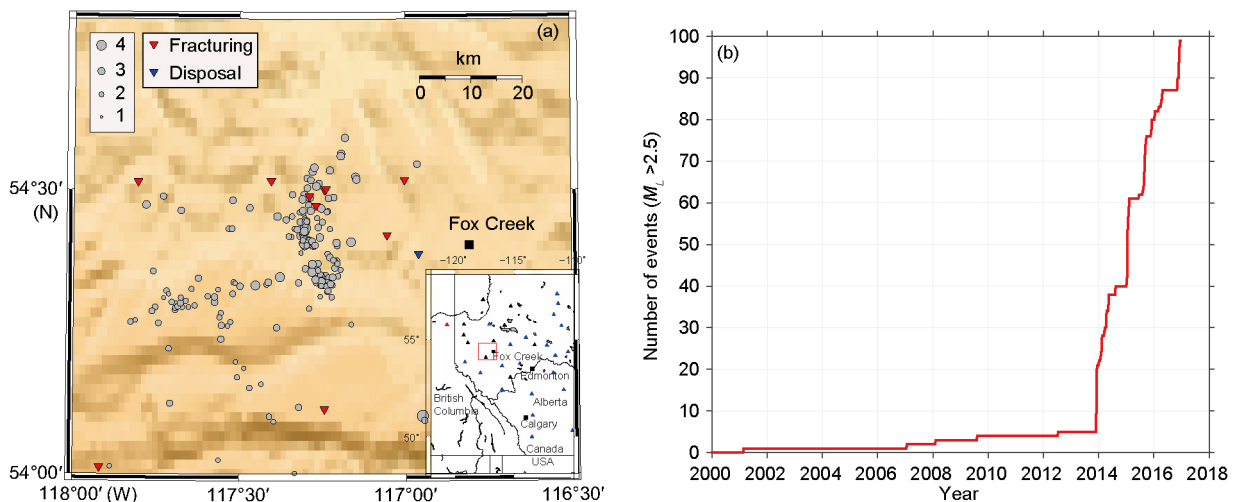
Figure 2   Seismicity near Fox Creek, Alberta, Canada. (a) Earthquake epicenters from the Canadian National Seismograph Network (CNSN), 2005–2016. There were no CNSN cataloged events in this area 1985–2005. Inverted triangles show the locations of hydraulic fracturing (red) and waste water disposal (blue) wells that have been identified being associated with $M>3$ earthquakes in the study by Atkinson et al. (2016). Inset shows the location of Fox Creek area, and regional seismic stations (triangles, blue: CRANE, black: Raven, red: CNSN). (b) Cumulative number of earthquakes with $M_L>2.5$ (excluding blast events) within 100 km radius from Crooked Lake (54.45°N, 117.25°W). Hydraulic fracturing started in March 2010 in this area, with the first induced earthquake reported in December 2013.
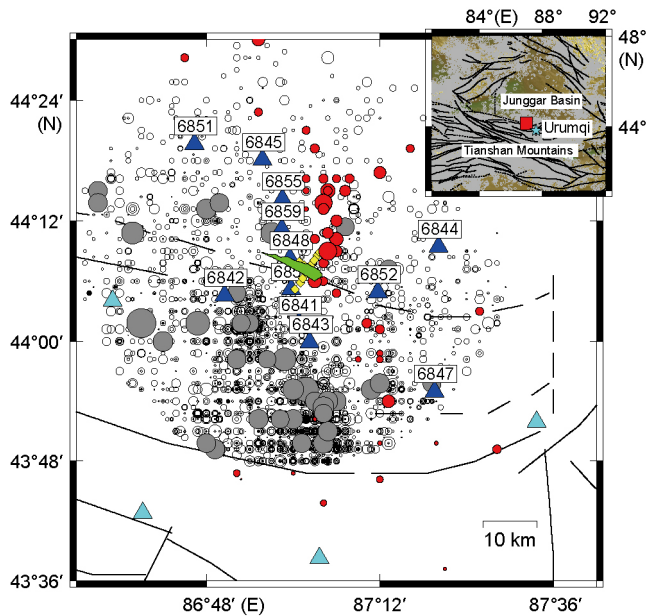
Figure 3 Map showing faults (lines), seismicity (circles), and seismic (triangles) and GPS (yellow diamonds) stations in the vicinity of the Hutubi gas repository (HGR) (green area). Grey dots denote the earthquakes with magnitudes larger than 3 since 1970. Red dots represent earthquakes occurred from June to August, 2013. Blue triangles are newly deployed seismic stations in 2013. Cyan triangles denote permanent stations operated by the Xinjiang Earthquake Administration. Zoom-in map showing location of the HGR (red square), faults (lines), and seismicity (grey dots) in Xinjiang.

ever, serious concerns were raised on the risk of induced seismicity, especially in the confining units for a geologic repository of supercritical CO_2 (Zoback and Gorelick, 2012). In a recent study, Gan and Frohlich (2013) reported an instance where the injection of CO_2 has triggered earthquakes with magnitudes 3 and larger in the Cogdell oil field, Texas.

2.2   Ground deformation associated with fluid injection

Human activities can cause ground deformation. Examples include coal mining (Carnec et al., 1996; Haynes et al., 1997), extracting petroleum and gas (Massonnet et al., 1997; Fielding et al., 1998), extracting groundwater (Galloway et al., 1998; Amelung et al., 1999), and geothermal fluid production (Barbour et al., 2016). Geodetic methods, especially GPS and InSAR (Interferometric Synthetic Aperture Radar) have been widely used to measure the scale, magnitude, and rate of the ground deformation (Massonnet and Feigl, 1998; Rosen et al., 2000; Bürgmann et al., 2000).

The wastewater disposal and injection of gas can potentially create some measurable surface deformation, due to either the expansion of the reservoir caused by the extra fluid or the induced fault slip, including aseismic slip and earthquakes. For instance, wastewater injection has caused vertical uplift, which was measured by InSAR images near several disposal wells in eastern Texas (Shirzaei et al., 2016). The large injection volume (7×10^5–9×10^5 m^3/year) and

the long operation period (2005–2007) may be the major factors for causing the line-of-sight (LOS) uplift rate up to 3 mm/year. Based on local geological profiles and hydraulic properties, the pore pressure increase due to injection is estimated to be around 0.5 to 1.5 MPa at the hypocentral depth of the 2012 M_w4.8 earthquake (Shirzaei et al., 2016), the largest among a sequence of seismicity between two closely spaced disposal wells and ~20 km from the area of largest uplift rate inferred from InSAR observations. In another example, InSAR measurements show surface uplift and subsidence in heavy oil fields in Alberta, Canada, and the deformation is highly correlated with the stimulation and extraction phases of cyclic steam operation (Granda et al., 2012; Samsonov S, private communication). InSAR images also detected ground deformation at a CO_2 sequestration site in southeast Saskatchewan, Canada (Samsonov et al., 2015).

However, at several locations of gas injection in Australia, Algeria, and Utah, USA, InSAR measurements have shown surface uplift of several cm, but in each case no earthquakes larger than magnitude of zero have been recorded (Gan and Frohlich, 2013). Whether the difference stems from the gas and liquid injection remains unknown. Another case is from the Hutubi natural gas repository in Xinjiang, China, where earthquakes occur immediately after the gas injection. Measurements of campaign GPS show ground deformation, but other factors such as underground water extraction and seasonal variation pose significant challenge to pinpoint the contribution from gas injection to the surface deformation (Wang D et al., 2016).

Surface deformation directly caused by induced earthquakes has been reported for the 2011 M_w5.3 Trinidad earthquake in Colorado (Barnhart et al., 2014), the 2016 M_w5.8 Pawnee earthquake in Oklahoma (Yeck et al., 2017; Fielding et al., 2017; Grandin et al., 2017; Pollitz et al., 2017), and the 2016 M_w5.0 Cushing earthquake in Oklahoma (Barnhart and Yeck, 2017). For the 2011 Trinidad earthquake, line-of-sight deformation over 6 cm was observed in InSAR data from the European Space Agency (ESA)'s Envisat satellite. Geodetic inversion suggests that the earthquake ruptured an 8–10 km long segment of a normal fault at depths of 1.5–6.0 km within the crystalline Precambrian basement underlying the Raton Basin sedimentary rocks (Barnhart et al., 2014). For the 2016 Pawnee earthquake, a region of line-of-sight shortening about 3 cm adjacent to the Pawnee main shock without surface rupture was shown in InSAR data from ESA's Sentinel-1A and -1B C-band radars and Canadian Radarsat-2 satellite. The general pattern of deformation is consistent with a shallow blind left-lateral strike-slip earthquake. The depth of maximum slip varies between slip models at 5.6, 7, and 12 km in Pollitz et al. (2017), Grandin et al. (2017), and Fielding et al. (2017), respectively. The variation might reflect the non-uniqueness in geodetic inversion and different choices of smoothing.

For the 2016 Cushing earthquake, the deformation signal is even clearer than that of the Pawnee earthquake, likely due to the shallow hypocentral depth and low atmospheric noise of InSAR data (Barnhart and Yeck, 2017). In contrast, there was no report of deformation observation for the 2011 M_w 5.7 Prague earthquake (Keranen et al., 2014) or the 2016 M_w 5.1 Fairview in Oklahoma (Barnhart et al., 2017). The lack of observed deformation for the 2011 Prague earthquake is surprising because the magnitude is similar to the Pawnee earthquake and its focal depth of 3.1 km (Sumy et al., 2014) is even shallower than the 4.7 km depth of the Pawnee earthquake (Yeck et al., 2017). The lack of deformation observation of the Prague earthquake is probably due to the small number of available InSAR satellite in the orbit and small number of acquired data around 2011. We expect to see more reports on deformation caused by the triggered earthquakes around the world considering the wide-spreading practice of hydraulic fracturing and wastewater disposal.

3.   Mechanism of induced earthquakes

3.1   Fluid diffusion and poroelasticity

Earthquake triggering due to external stress perturbations are commonly explained using the Coulomb failure criterion (Harris, 1998; Steacy et al., 2005), where the Coulomb Failure Stress change is defined as

$$\Delta \mathrm{CFS} = \Delta \tau - \mu \Delta(\sigma - p), \tag{1}$$

here $\Delta\tau$ and $\Delta\sigma$ are shear (positive in slip direction) and normal (positive in compression) stress changes, respectively, resolved onto a certain fault orientation; Δp is the pore pressure change, and μ is the dry friction coefficient on the fault, which usually ranges from 0.6 to 0.8. The difference between normal stress and pore pressure is defined as the effective normal stress $\Delta\bar{\sigma} = \Delta(\sigma - p)$. A positive Coulomb stress change (ΔCFS>0) promotes fault failure whereas a negative ΔCFS prohibits failure.

Figure 4 illustrates two plausible ways that fluid injection may affect the Coulomb stress and promote failure. First, fluid injection can lead to pore fluid diffusion along newly created fractures and/or pre-existing fault zones, temporally increase pore pressure hence reduce the effective normal stress, and bring a pre-existing fault or intact rock close to failure. It has long been postulated as a leading mechanism for earthquakes induced by oil and gas extractions (e.g., Hubbert and Rubey, 1959; Healy et al., 1968; Raleigh et al., 1976). Seismicity directly induced by pore pressure increase has been documented for both hydraulic fracturing and wastewater disposal scenarios. For example, seismic swarm activity has been reported during the hydraulic fracturing from a vertical borehole in the Barnette Shale formation
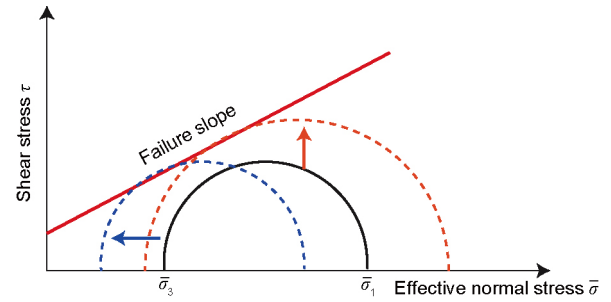
Figure 4   Two possible mechanisms fluid injection may induce earthquakes. Mohr Circle representations of stress state before perturbation (black, solid), after homogeneous pore pressure increase (effective normal stress decrease) (blue, dashed), and after solid matrix stress (shear and/or normal) changes (orange, dashed). Cohesion and friction coefficient are assumed to be constant before and after perturbation.

of the Fort Worth Basin (Fisher et al., 2004) as a result of fast fluid diffusion due to enhanced formation permeability (Shapiro and Dinske, 2009). In Oklahoma, fluid migration from high-rate disposal wells may be responsible for the rapid increase in seismicity in Oklahoma, and suggested regular reservoir pressure monitoring as means of hazard assessment (Keranen et al., 2014).

Second, fluid injection can directly perturb the solid matrix stresses (shear and normal) in the surrounding media and bring faults with preferred orientations closer to failure. This scenario does not necessarily require an increase in pore pressure, and may be particularly effective under hydraulic fracturing operations and extraction of fluids (Rudnicki, 1986; Segall, 1989; Segall and Lu, 2015; Deng et al., 2016; Chang and Segall, 2016). While wastewater disposal can last for years to decades, each stage of hydraulic fracturing typically lasts for a few hours, and each horizontal well is completed within a couple of weeks. Thus, the direct pore pressure increase may not be as significant on such short time scales, due to the low permeability of the shale formation. Recent studies of induced earthquakes in the western Canada sedimentary basin (WCSB) have found that most recent cases of induced earthquakes (2010-2015) of *M*>3 are highly correlated in space and time with hydraulic fracturing, in contrast to deep disposal of coproduced wastewater for induced seismicity in the central US (Schultz et al., 2015; Atkinson et al., 2016; Bao and Eaton, 2016; Schultz et al., 2017). Although the differences in the total injection volume in disposal wells (sometimes up to 100 times) can play a role (Schultz et al., 2014; Mahani et al., 2017), the distinction between instantaneous solid matrix stress changes that are most effective during and shortly after hydraulic fracturing treatment and long-term pore pressure buildup from fluid diffusion may also be a key factor in the different correlations in central US and WCSB. To test this idea, Deng et al. (2016) developed a poroelasticity model for calculating the fully coupled solid matrix stress changes and fluid pressure diffusion in an anisotropic media due to multi-stage stimulation

and successfully explained the spatiotemporal distribution of an induced earthquake sequence in December 2013 near Fox Creek, Alberta, Canada. Their modeling results demonstrated that during the hydraulic fracturing the solid matrix stress changes on a pre-existing fault located 1–2 km from the horizontal well far exceed the pore pressure increase, and most of the seismicity in the December 2013 sequence is spatiotemporally correlated with the positive regime of the resulting Coulomb stress change. The poroelasticity model thus suggests, due to low permeability of shale formation, shear stress accumulation rather than diffusion of pore pressure is more likely the dominant factor bringing critically stressed medium to failure (Deng et al., 2016). Near-instantaneous stress redistribution caused by poroelastic coupling has also been suggested as the triggering mechanism for two cases of hydraulic fracturing induced seismicity in Ohio, inferred from the temporal correlation of either a maximum count of seismicity or the largest magnitude event reported during the fracking treatment (Friberg et al., 2014; Skoumal et al., 2015). A recent study on remote dynamic triggering in three sedimentary basins in Canada, where recent fluid injection is correlated with increasing seismicity, also suggests that susceptibility to triggering and the mechanism of instantaneous versus delayed triggering may be related to the relative influences from pore pressure and solid matrix stress changes (Wang et al., 2015). Future poroelastic stress modeling work using realistic injection history, formation permeability structure and fault orientation is needed to quantitatively verify the casual relation.

3.2 Maximum magnitude

One of the most critical issues of induced seismicity hazard assessment is whether there exists a magnitude-predictable relationship between operation parameters (i.e., total injection volume, volume rate, wellhead pressure, etc.) and induced events, and if yes how to develop such a relationship. While a fundamental step in the development of such a relationship relies on the understanding of the physical processes of induced earthquakes, first-order estimates on the maximum magnitude have been explored by several studies (e.g., McGarr, 2014; Dieterich et al., 2015; Ampuero et al., 2016). Each of these estimates involves a set of assumptions about the source processes, some of which appear plausible but are difficult to prove. For example, McGarr (2014) derived that the maximum moment of an induced earthquake is proportional to the total injection volume $M_0(\max)=G\Delta V$ (G is shear modulus, ΔV is injection volume), by assuming that (1) induced earthquakes have shear stress drops proportional to the pore pressure increase calculated from the injected fluid volume, (2) induced seismicity follows the Gutenberg-Richter magnitude-frequency distribution, and (3) the strain change within a defined volume is proportional to the cumulative

moment of all earthquakes in that volume (Kostrov, 1974). A similar scaling of $M_w \sim \log_{10}(V)$ is derived by Dieterich et al (2015) from a different line of reasoning, assuming that the volume of the pressurized crust V would be proportional to the injected volume ΔV at least during the initial injection period. Although the above relationship initially agrees with data from some wastewater disposal, fracking and enhanced geothermal wells, more recent studies clearly showed that some WCSB fracking induced earthquakes have seismic moments up to 100 times of the McGarr's upper limit prediction, despite their small to moderate total injection volumes compared to those in disposal wells (British Colombia Oil and Gas Commission, 2015; Atkinson et al., 2016). Another statistical study on induced seismicity in the US mid-continent also found the injection rate of a well, rather than its total injection volume or monthly wellhead pressure, is much more strongly associated with seismicity, and suggested that management of well injection rates could be a useful tool in reducing potential induced seismic hazard (Weingarten et al., 2015). Depending on the relative distances between the wells and receiver faults, stress perturbations from multiple wells can make cumulative contributions to promoting fault instability (Walsh and Zoback, 2016).

Alternatively, van der Elst et al. (2016) suggested that, while the total number of induced earthquakes may be related to the injection parameters, once the fluids permeate to a pre-existing fault and promote seismic slip on it, the maximum magnitude of such earthquakes should follow the Gutenberg-Richter magnitude-frequency distribution assuming no upper bound. The distinction between the two hypotheses for the maximum magnitude lies exactly on the induced earthquake source processes, in that the McGarr (2014) and Weingarten et al. (2015) model assumes events occur in the vicinity of the injection sources whereas the van der Elst et al. (2016) model assumes tectonics plays a more important role in controlling how large the earthquakes can potentially grow, although the nucleation may be due to fluid injection.

4.   Public and regulatory polices

4.1   Impact of induced earthquakes on short-term seismic hazard maps

Ground motion prediction plays a crucial role in seismic hazard assessment and preparation. Consequently, it is intriguing to investigate whether induced earthquakes produce similar ground shaking as natural events do. Using spatially rich intensity data from the USGS "Did You Feel It" system, Hough (2014) suggested that induced earthquakes have lower effective intensity magnitude than natural earthquakes in the central and eastern US (CEUS), indicating that less ground shaking will be generated by induced earthquakes than tectonic

earthquakes, despite of shallower focal depths of the former.

Another intriguing yet critical question is how to incorporate the recent occurrences of induced seismicity into the national earthquake hazard map based on probabilistic analysis (Petersen et al., 2015). After considering the recent short-term (2014-15) seismicity rates and assuming the activity rate will remain stationary over next year, the updated one-year hazard map shows significant impact from the induced earthquakes in that hazard is 3- to 10-fold higher near some areas of active induced earthquakes than in the 2014 USGS National Seismic Hazard Model, which did not consider induced earthquakes (Petersen et al., 2016). A striking feature is that in the 2016 one-year model of Modified Mercalli Intensity (MMI) the 1% probability of exceedance in one year appears to be higher in Oklahoma than the long recognized New Madrid Seismic Zone in central US, highlighting the necessity of taking into account of induced earthquakes for seismic hazard assessment.

4.2   Traffic light protocols

Given the global increasing energy demand, anthropogenic processes that can induce earthquakes seem inevitable. A proper protocol of such anthropogenic processes is necessary to reduce the potential damage and property losses by the induced earthquakes. A "traffic light" system is a seismic hazard management plan that the industry and government regulators develop for their decision-making process in response to the occurrence of earthquakes associated with anthropogenic activities.

Traffic light protocols (TLP) for induced seismicity was first proposed for regulations of hydraulic stimulations of geothermal systems (Bommer et al. 2006), where the peak ground velocity (PGV), induced earthquake magnitude, and seismicity rate are all considered in the determination of the "traffic lights". For example, the TLP developed for the enhanced geothermal operations in Basel, Switzerland, consists of 4 levels, green, yellow, orange, and red, moving up the scale as the above criteria exceed certain preset thresholds and corresponding action plans by the industrial operators and government regulators (Häring et al., 2008). A green light is issued when PGV < 0.5 mm/s, local magnitude M_L < 2.3, and there are no felt reports. A yellow light is given when PGV ≤ 2.0 mm/s, M_L ≥ 2.3 and few felt reports. Operators need to inform regulators and stop increasing pumping rate. An orange light is given when PGV ≤ 5 mm/s, M_L ≥ 2.9 and many felt reports. In such a case, the operators must reduce wellhead pressure by decreasing pumping or by bleeding the well. When PGV exceeds 5 mm/s and local magnitude is greater than 2.9 with generally felt reports, pumping must stop and wells need to be kept at the minimum wellhead pressure (Häring et al., 2008). The criteria and cut-off thresholds used in TLP for different types of operations vary considerable in different regions and countries. Table 1 summarizes the TLPs currently in practice in Europe and North America (Kao et al., 2016).

Table 1   Summary of Traffic light protocols (TLP) currently in practice in Europe and North America[a]

Country/State/Province	PGV (mm/s)	M_L	Felt reports	TLP
Basel, Switzerland	< 0.5	< 2.3	No	Green
	≤ 2.0	≥ 2.3	Few	Yellow
	≤ 5.0	≥ 2.9	Many	Orange
	> 5.0	> 2.9	General area	Red
UK		≥ 0.0		Yellow
		≥ 0.5		Red
Colorado, US			Felt at surface	Yellow
		> 4.5		Red
Ohio, US		Buffer zones around high risk areas		Yellow
		≥ 1.0		Red
Oklahoma, US		Areas of interest (10 km from any M4+ events or M3+ swarms)		Yellow
		≥ 1.8 to 3.7*		Red
Alberta, Canada		≥ 2.0		Yellow
		≥ 4.0		Red
British Columbia, Canada		≥ 4.0		Red

a) Modified from Kao et al. (2016). In general, a "yellow" light requires the operators to modify operation parameters (e.g., pumping rate, wellhead pressure). Operations must stop under a "red" light. *Exact TLP thresholds are determined on a well-to-well basis (Wong et al., 2015).

5.   Discussion and perspective

5.1   Source properties and seismicity patterns of induced and natural earthquakes

Despite the recent progress on the induced earthquakes, it is still challenging to reliably discriminate injection-induced (anthropogenic) and natural (tectonic) earthquakes. The source parameter approach has been shown to be effective in making direct comparisons between individual events. In practice, earthquake source properties, focal mechanism and stress drop can provide insights to the faulting process that generated the seismic event.

While most tectonic earthquakes have nearly pure double-couple (DC) moment tensor solutions, some earthquakes related to fluids of either natural or anthropogenic causes are reported to have significant non-DC components due to complex local fracturing processes. For example, mixed non-double-couple and shear motions have been inferred for volcanic earthquakes (Julian et al., 1998) and events accompanied by rapid fluid flow during crack opening in geothermal fields (Guilhem et al., 2014). A recent study using full waveform inversion also found that eight $M_w \geq 3.5$ induced earthquakes in the WCSB have significant isotropic and CLVD components, with the 2015/06/13 M_w4.1 Fox Creek event reaching a combined ISO and CLVD of 70% (i.e., only 30% DC component) (Zhang et al., 2016). Such large non-DC source mechanisms can arise from a variety of processes including the activation of multiple, sub-parallel shear fractures due to high pressure during injection, the creation of damage and rock porosity change caused elastic moduli variations, or combined effects of the above factors. However, we note that having a significant non-DC component in the moment tensor solution is not a sufficient condition for discriminating injection-induced versus tectonic events. Complex local fracturing process can result in large non-DC components for tectonic earthquakes such as in a volcanic system (Julian et al., 1998), meanwhile induced earthquakes on pre-existing faults may exhibit primarily DC focal mechanism (McNamara et al., 2015). For example, another M_w4.1 Fox Creek event on 2016/01/12 was shown to have limited non-DC component (~22%) (Wang et al., 2017).

Static stress drop, the shear stress change on a fault before and after an earthquake, might shed light on the different source processes of induced and natural earthquakes. Hough (2014) suggested that the stress drop of induced earthquakes in CEUS may be lower than their tectonic counterparts, although this study used USGS ground shaking intensity distribution as a proxy for stress drop values. In contrast, two recent studies analyzing the spectra or spectra ratios of induced earthquakes in the WCSB have found that these events have stress drop values between 1 and 100 MPa (Zhang et al., 2016; Clerc et al., 2016), within the range and even

on the high end of typical tectonic earthquake stress drops (0.1–100 MPa). Stress drop estimates often have notoriously large uncertainties due to attenuation along the wave path, site responses, and the ambiguities in applying different spectra models to fit the corner frequencies. While influence of the first two factors may be alleviated with the empirical Green's function approach, the last factor persists and makes it challenging to compare the face values of stress drops from individual studies. Accurate estimates of stress drops of different types of induced earthquakes and appropriate comparison to tectonic earthquakes from the same geographic region are thus key to future research on the source properties of induced seismicity.

In addition to the efforts to discriminate induced and natural earthquakes from their source properties, seismicity pattern analysis has been used to investigate induced earthquakes. The first approach is to find the difference between natural and induced seismicity by using some summarizing statistics. For example, Bachmann et al. (2012) found that the *b*-value in the magnitude-frequency relation is correlated to pore-pressure: the *b*-value decreases from the co-injection period to the post-injection period as well as decreases with the distance to the injection points. Using clustering analysis, Zaliapin and Ben-Zion (2016) studied features of induced earthquakes in the Geyser geothermal field in northern California and TauTona gold mine in South Africa, and compared to seismicity from some regular tectonic zones. They found several distinguishing characteristics of induced seismicity, such as higher rate of background events, faster temporal decay of clusters, higher rate of repeating events, larger proportion of small clusters, and larger spatial separation from the initiating event and other events in a cluster. These conclusions need to be verified by further studies.

5.2   Statistical and physics-based seismicity models

Statistical analysis on short-term seismicity such as the Epidemic-Type Aftershock Sequence (ETAS) model (e.g. Ogata, 1988; Ogata, 1998; Zhuang et al., 2002; Ogata and Zhuang, 2006) have been widely used for modelling the short-term earthquake clustering behavior and producing daily forecasts (e.g., Zhuang, 2011). The theories and techniques related to the ETAS model have been utilized to study induced seismicity (e.g. Llenos and Michael, 2013; Llenos and Michael, 2016). Using the change-point detection technique proposed by Ogata (1988), Llenos and Michael (2013) found changes in the background seismicity rate and triggering parameters in both Oklahoma and Arkansas, and concluded that swarms that occurred following fluid injection differ from swarms triggered by natural processes. Such changes were also confirmed by Wang P et al. (2016) and Gupta and Baker (2015) by using approaches of Bayesian model comparison. By fitting ETAS model to seismicity data from the Basel EGS sites,

Switzerland, Bachmann et al (2011) have found that the background seismicity rate shows good correlation with the pumping history in each time window. Using similar methods, Eto et al. (2013) draw the same conclusion for induced seismicity in the Yanizu-Nishiyama hydrothermal field, Japan. One key point of such statistical approach is to robustly estimate the background seismicity rate, which can be obtained from different methods, such as specifying background rate (e.g. Imoto, 2001), stochastic reconstruction method (Hainzl and Ogata, 2005; Hainzl et al., 2016), and using Bayesian analysis with smoothness prior (e.g., Ogata et al., 2003; Kumazawa and Ogata, 2014). To date, the Bayesian analysis, which has been shown powerful in detecting the changes of seismicity patterns due to known or unknown causes in the study of natural earthquakes (e.g., Ogata et al., 2003) or volcano induced swarms (Kumazawa et al., 2016), has not yet been introduced in the study of fluid injection induced seismicity.

Furthermore, comprehensive system-level models that couple physics-based simulations of seismicity with reservoir simulations of fluid pressure changes can provide an experimental capability to investigate topics related to induced seismicity (Dieterich et al., 2015). Using an earthquake simulator based on rate-state friction including injection history that leads to pore pressure variation over time, Dieterich et al., (2015) find that the spatial-temporal patterns of simulated injection-induced seismicity are quite sensitive to pre-injection fault stresses. Moreover, continuing seismicity following shut-in of injection appears to be driven primarily by delayed nucleation and decays by the Omori aftershock law. Although the initial work was done on an extremely simple fault and injection system (Dieterich et al., 2015), it lays out the foundation to target specific cases by incorporating realistic injection history, reservoir and fault geometry, as well as hydraulic properties.

5.3   Near-field and *in situ* observations

While many of fluid injection induced earthquakes occur in regions of seismic quiescence prior to oil and gas operations, the relatively sparse seismographic network in such areas may play a role in the lack of full characterization of nearby natural earthquakes. Numerous examples have underscored the importance of good network coverage for elucidating high-resolution spatial-temporal evolution of seismicity. For instance, seismicity recorded by the sparse regional network near the Hutubi gas repository usually has large uncertainties in locations (Zhang et al., 2017). Without mapping out in high resolution the local seismicity near injection sites, it is extremely difficult to understand by what mechanisms the fluid injection may cause earthquakes. Another challenge is that usually a significant portion of seismicity is missing by seismic network due to signal-noise-ratio of waveforms. Such small magnitude events can be detected by advanced

event detection algorithms such as the matched filter technique (Yang et al., 2009).

Even though we can improve the seismic network coverage rapidly, it is not sufficient to elucidate the mechanism of how fluid may trigger fault slip without in-situ observations. One recent experiment in France, the step-rate injection method for fracture in situ properties (SIMFIP), is probably the only case where triggered fault slip is directly observed. In the SIMFIP experiment a preexisting fault cutting through a carbonate formation accessible for examination and instrumentation was selected, allowing the simultaneous measuring of fault-normal displacements, fault-parallel displacements, and fluid pressure after fluid injection (Guglielmi et al., 2015a, b; Cornet, 2016). The authors observe highly dilatant and slow aseismic slip associated with reduced dilatancy and micro-earthquakes. Most aseismic slip occurs within the fluid-pressurized zone and obeys a rate-strengthening friction law. Fluid injection primarily triggers aseismic slip in this experiment, with micro-earthquakes being an indirect effect mediated by aseismic creep. This poses another significant question on how the fluid injections may promote fault slip, aseismic or seismic.

To tackle such challenges not only demands more in situ observations, which may be conducted by drilling projects involving multidisciplinary approaches, but also demands better understanding of how fault zone properties may be altered by injected fluids and control fluid migration. A fault zone (FZ) usually includes a fault core and the surrounding damage zone with highly fractured materials (e.g. Chester et al., 1993). Whether the fault zone acts as a conduit, a barrier, or a conduit-barrier combined system for fluids is determined by the grain-scale permeability of the fault core and the hydraulic properties of the fracture network in the damage zone (Caine et al., 1996). It has been suggested to use the ratio between the damage zone width and the fault zone width (damage zone width + fault core width) to quantify the barrier-to-conduit permeability structure (Caine et al., 1996), providing a plausible way to estimate the permeability structure of faults near the fluid injection points. In general the seismically observed damage zone is much wider than the fault core (e.g. Yang, 2010, 2015), and thus the fluid flow properties of the fault damage zone primarily controls how the fluid injection may promote slip on the fault. Excluding exhumed faults or FZ drilling projects, the damage zone structure is mostly quantified by modeling fault zone related waves, such as trapped waves (e.g. Li et al., 1990) and FZ-reflected body waves (e.g. Yang and Zhu, 2010; Yang et al., 2011, 2014). Most recently discovered damage zones extend to a shallow depth, 2–5 km below the surface (e.g. Yang and Zhu, 2010; Yang, 2015) and may exhibit along-strike variations (e.g. Yang et al., 2014). The damage zones reflect past rupture behaviors, and could promote future earthquake rupture propagation (Weng et al., 2016). Although high-resolu-

tion imaging of fault zone structure has been well developed, monitoring how the fault zone evolves over time in the field is still one of challenges in earthquake physics (Yang, 2015). In addition to the growing dense array deployments, high-quality repeating active sources (Wang et al., 2012) may advance our ability to continuously monitor temporal changes of fault zones at depth and thus provide critical keys in understanding how fluid injection may induce earthquakes.

5.4   Collaboration between academia, industry and government

The issue of induced seismicity is politically and emotionally charged. There is a delicate balance between the positive economic impacts of resource development and the public's concerns about the potential environmental impact of the infrastructure buildup, environmental contamination, and induced seismicity. The acquiring and preserving of "social licenses" for drilling and injection requires transparent translation from independent scientific knowledge to regulatory policies and operation protocols. A collaborative relationship among academia, industry and government, is crucial.

Geological Survey of Canada (GSC) launched the Induced Seismicity Research (ISR) project in 2012 under the Environmental Geoscience Program. One of the mandates of ISR is to provide scientific information to all levels of government for making public policies in the development of unconventional oil and gas and protection of public safety and environment. GSC has organized workshops in 2015 and 2016 with attendees from industry, government and academia to facilitate direct dialogs and collaborations (Kao et al., 2016). Regional seismic network coverage has been increasingly densified in the past few years in northeast British Columbia and Alberta to expand monitoring capability of induced earthquakes, through the joint effort of the federal and provincial government. Local dense arrays focusing on specific injection wells are also installed, including some stations directly on company properties, as research project based temporary deployments. Permanent regional station data are open to the public and individual PI based local array data are typically open after certain embargo periods. In addition, industrial operators are encouraged to share part of their private station data with academic researchers under confidential research agreements. All the above channels for collaboration have stimulated the induced seismicity research in Canada in the recent years.

Similar types of dialogues have taken place in the United States, such as the induced seismicity workshop co-hosted by the U.S. Geological Survey (USGS) and Oklahoma Geological Survey in 2014, during which participants from academia, industry and government discussed research agenda for incorporating induced seismicity in the US National Seismic Hazard Model (NSHM) and essentially laid the groundwork for the development of the 2016 USGS one-year, regional seismic hazard map (Petersen et al., 2015; Petersen et al., 2016). Numerous reports have been published as a result of close collaborations between academia, industry and government. For example, the US Environmental Protection Agency has published a report with the title "Minimizing and Managing Potential Impacts of Injection-Induced Seismicity from Class II Disposal Wells: Practical Approaches" in February 2015. This report has been peer reviewed by experts from both industry and academia.

Currently, data sharing is the major challenge in the collaboration. Researchers need access to a full range of data, especially injection parameters and near-field seismograms from the industry to understand induced seismicity. However, because such datasets include embedded proprietary details, the industry would need strong incentives to agree to share with academic researchers and government agencies. Finding a protocol that will allow data sharing but also protect industrial proprietary information will be the next step stone towards understanding induced seismicity. This requires close and frequent conversations between all the stakeholders, including industry, academia, government, and the general public. Recently, the Canadian Association of Petroleum Producers (CAPP) has formed the Induced Seismicity Task Group, with 12 companies participating. The group has a mandate to "engage in deep sharing of industry best practices in mitigation and management of induced seismicity risk from hydraulic fracturing." Looking to the future, we hope a proper framework of operating guidelines and procedures will result from close collaborations.

References

Amelung F, Galloway D L, Bell J W, Zebker H A, Laczniak R J. 1999. Sensing the ups and downs of Las Vegas: InSAR reveals structural control of land subsidence and aquifer-system deformation. Geology, 27: 483

Ampuero J P, Galis M, Mai P M. 2016. Physics-based estimates of maximum magnitude of induced earthquakes. Geophys Res Abstracts, 18: EGU2016-9371, EGU General Assembly

Atkinson G M, Eaton D W, Ghofrani H, Walker D, Cheadle B, Schultz R, Shcherbakov R, Tiampo K, Gu J, Harrington R M, Liu Y, van der Baan M, Kao H. 2016. Hydraulic fracturing and seismicity in the western Canada sedimentary basin. Seismol Res Lett, 87: 631–647

Bao X, Eaton D W. 2016. Fault activation by hydraulic fracturing in western Canada. Science, 354: 1406–1409

Mahani A B, Schultz R, Kao H, Walker D, Johnson J, Salas C. 2017. Fluid Injection and Seismic Activity in the Northern Montney Play, British Columbia, Canada, with Special Reference to the 17 August 2015 M_w 4.6 Induced Earthquake. Bull Seismol Soc Am, 107: 542–552

Bachmann C E, Wiemer S, Woessner J, Hainzl S. 2011. Statistical analysis of the induced Basel 2006 earthquake sequence: Introducing a probability-based monitoring approach for Enhanced Geothermal Systems. Geophys J Int, 186: 793–807

Bachmann C E, Wiemer S, Goertz-Allmann B P, Woessner J. 2012. Influence of pore-pressure on the event-size distribution of induced earthquakes. Geophys Res Lett, 39: L09302

Barbour A J, Evans E L, Hickman S H, Eneva M. 2016. Subsidence rates at the southern Salton Sea consistent with reservoir depletion. J Geophys Res-Solid Earth, 121: 5308–5327

Barnhart W D, Benz H M, Hayes G P, Rubinstein J L, Bergman E. 2014. Seismological and geodetic constraints on the 2011 M_w 5.3 Trinidad, Colorado earthquake and induced deformation in the Raton Basin. J Geophys Res-Solid Earth, 119: 7923–7933

Barnhart W D, Yeck W L. 2017. InSAR constraints on recent induced earthquakes in the United States. Seismological Society of America Annual Meeting, 18–20 April, Denver, Colorado

Bommer J J, Oates S, Cepeda J M, Lindholm C, Bird J, Torres R, Marroquín G, Rivas J. 2006. Control of hazard due to seismicity induced by a hot fractured rock geothermal project. Eng Geol, 83: 287–306

British Colombia Oil and Gas Commission (BCOGC). 2012. Investigation of Observed Seismicity in the Horn River Basin. British Columbia Oil and Gas Commission Report. 29

British Colombia Oil and Gas Commission (BCOGC). 2015. August Seismic Event Determination. Industry Bulletin 2015-32, https://www.bcogc.da

Brodsky E E, Lajoie L J. 2013. Anthropogenic seismicity rates and operational parameters at the Salton Sea geothermal field. Science, 341: 543–546

Bürgmann R, Rosen P A, Fielding E J. 2000. Synthetic aperture radar interferometry to measure Earth's surface topography and its deformation. Annu Rev Earth Planet Sci, 28: 169–209

Carnec C, Massonnet D, King C. 1996. Two examples of the use of SAR interferometry on displacement fields of small spatial extent. Geophys Res Lett, 23: 3579–3582

Caine J S, Evans J P, Forster C B. 1996. Fault zone architecture and permeability structure. Geology, 24: 1025–1028

Chang K W, Segall P. 2016. Injection-induced seismicity on basement faults including poroelastic stressing. J Geophys Res-Solid Earth, 121: 2708–2726

Chester F M, Evans J P, Biegel R L. 1993. Internal structure and weakening mechanisms of the San Andreas Fault. J Geophys Res, 98: 771–786

Clerc F, Harrington R M, Liu Y, Gu Y J. 2016. Stress drop estimates and hypocenter relocations of induced seismicity near Crooked Lake, Alberta. Geophys Res Lett, 43: 6942–6951

Cornet F H. 2016. Seismic and aseismic motions generated by fluid injections. Geomechanics Energ Environ, 5: 42–54

Deng K, Liu Y, Harrington R M. 2016. Poroelastic stress triggering of the December 2013 Crooked Lake, Alberta, induced seismicity sequence. Geophys Res Lett, 43: 8482–8491

Dieterich J H, Richards-Dinger K B, Kroll K A. 2015. Modeling injection-induced seismicity with the physics-based earthquake simulator RSQSim. Seismol Res Lett, 86: 1102–1109

Ellsworth W L. 2013. Injection-induced earthquakes. Science, 341: 1225942

Evans D M. 1966. The Denver area earthquakes and the Rocky Mountain Arsenal disposal well. Mountain Geologist, 3: 23–26

Eto T, Asanuma H, Adachi M, Saeki K, Aoyama K, Ozeki H, Mukuhira Y, Häring M 2013. Application of the ETAS seismostatistical model to microseismicity from geothermal fields. GRC Transactions, 37: 149–154

Fielding E J, Blom R G, Goldstein R M. 1998. Rapid subsidence over oil fields measured by SAR interferometry. Geophys Res Lett, 25: 3215–3218

Fielding E J, Sangha S S, Bekaert D P S, Samsonov S V, Chang J C. 2017. Surface deformation of north-central Oklahoma related to the 2016 M_w 5.8 Pawnee Earthquake from SAR interferometry time series. Seismol Res Lett, 88, doi: 10.1785/0220170010

Fisher M K, Heinze J R, Harris C D, Davidson B M, Wright C A, Dunn K P. 2004. Optimizing horizontal completion techniques in the Barnett Shale using microseismic fracture mapping: Proceedings of the Society of Petroleum Engineers Annual Technical Conference, Houston, Texas. SPE Paper 90051, 11

Friberg P A, Besana-Ostman G M, Dricker I. 2014. Characterization of an earthquake sequence triggered by hydraulic fracturing in Harrison County, Ohio. Seismol Res Lett, 85: 1295–1307

Frohlich C. 2012. Two-year survey comparing earthquake activity and injection-well locations in the Barnett Shale, Texas. Proc Natl Acad Sci USA, 109: 13934–13938

Galloway D L, Hudnut K W, Ingebritsen S E, Phillips S P, Peltzer G, Rogez F, Rosen P A. 1998. Detection of aquifer system compaction and land subsidence using interferometric synthetic aperture radar, Antelope Valley, Mojave Desert, California. Water Resour Res, 34: 2573–2585

Gan W, Frohlich C. 2013. Gas injection may have triggered earthquakes in the Cogdell oil field, Texas. Proc Natl Acad Sci USA, 110: 18786–18791

Giardini D. 2009. Geothermal quake risks must be faced. Nature, 462: 848–849

Goertz-Allmann B P, Goertz A, Wiemer S. 2011. Stress drop variations of induced earthquakes at the Basel geothermal site. Geophys Res Lett, 38: L09308

Grandin R, Vallee M, Lacassin R. 2017. Rupture process of the Oklahoma M_w 5.7 Pawnee earthquake from Sentinel-1 InSAR and seismological data. Seismol Res Lett, 88, doi: 10.1785/0220160226

Granda J, Indreiten T, Sviland K M, Savage M, Arnaud A, Cooksley G, Bisects E. 2012. Ground motion monitoring with radar technology—Case study of SAGD operations of Leismer: Results of ground motion monitoring during first year of steam injection and preliminary comparison with reservoir performance data. World Heavy Oil Congress, WHOC12-211, Aberdeen, Scotland

Grigoli F, Cesca S, Priolo E, Rinaldi A P, Clinton J F, Stabile T A, Dost B, Fernandez M G, Wiemer S, Dahm T. 2017. Current challenges in monitoring, discrimination, and management of induced seismicity related to underground industrial activities: A European perspective. Rev Geophys, doi: 10.1002/2016RG000542

Guglielmi Y, Elsworth D, Cappa F, Henry P, Gout C, Dick P, Durand J. 2015a. In situ observations on the coupling between hydraulic diffusivity and displacements during fault reactivation in shales. J Geophys Res-Solid Earth, 120: 7729–7748

Guglielmi Y, Cappa F, Avouac J P, Henry P, Elsworth D. 2015b. Seismicity triggered by fluid injection-induced aseismic slip. Science, 348: 1224–1226

Guilhem A, Hutchings L, Dreger D S, Johnson L R. 2014. Moment tensor inversions of M ~3 earthquakes in the Geysers geothermal fields, California. J Geophys Res-Solid Earth, 119: 2121–2137

Gupta A, Baker J W. 2015. A Bayesian change point model to detect changes in event occurrence rates, with application to induced seismicity. ICASP12-12th International Conference on Applications of Statistics and Probability in Civil Engineering, Vancouver, Canada, 12–15 July 2015

Hainzl S, Ogata Y. 2005. Detecting fluid signals in seismicity data through statistical earthquake modeling. J Geophys Res, 110: B05S07

Hainzl S, Fischer T, Čermáková H, Bachura M, Vlček J. 2016. Aftershocks triggered by fluid intrusion: Evidence for the aftershock sequence occurred 2014 in West Bohemia/Vogtland. J Geophys Res-Solid Earth, 121: 2575–2590

Häring M O, Schanz U, Ladner F, Dyer B C. 2008. Characterisation of the Basel 1 enhanced geothermal system. Geothermics, 37: 469–495

Harris R A. 1998. Introduction to special section: Stress triggers, stress shadows, and implications for seismic hazard. J Geophys Res, 103: 24347–24358

Haynes M, Capes R, Lawrence G, Smith A, Shilston D, Nicholls G. 1997. Major urban subsidence mapped by differential SAR Interferometry. Proc. Third ERS Symp. Space Serv. Environ., Florence, Italy, 17–21 March, (ESA SP-414), 1: 573–577

Healy J H, Rubey W W, Griggs D T, Raleigh C B. 1968. The Denver earthquakes. Science, 161: 1301–1310

Hough S E. 2014. Shaking from injection-induced earthquakes in the central and eastern United States. Bull Seismological Soc Am, 104: 2619–2626

Hubbert M K, Rubey W W. 1959. Role of fluid pressure in mechanics of overthrust faulting: 1. Mechanics of fluid-filled porous solids and its application to overthrust faulting, porous solids and its application to overthrust faulting. Geol Soc Am Bull, 70: 115–166

Imoto M. 2001. Point process modelling of reservoir-induced seismicity. J Appl Probab, 38A: 232–242, doi: 10.1239/jap/1085496605

IPCC. 2005. Underground geological storage. In: Metz B, Davidson O, de Coninck H C, Loos M, Meyer L, ed. IPCC Special Report on Carbon Dioxide Capture and Storage. 195–276. Cambridge: Cambridge University Press

Julian B R, Miller A D, Foulger G R. 1998. Non-double-couple earthquakes 1. Theory. Rev Geophys, 36: 525–549

Kao H, Eaton D W, Atkinson G M, Maxwell S, Mahani A B. 2016. Technical meeting on the traffic light protocol (TLP) for induced seismicity: Summary and recommendations. Geological Survey of Canada, Open File 8075, doi: 10.4095/299002

Keranen K M, Savage H M, Abers G A, Cochran E S. 2013. Potentially induced earthquakes in Oklahoma, USA: Links between wastewater injection and the 2011 M_w 5.7 earthquake sequence. Geology, 41: 699–702

Keranen K M, Weingarten M, Abers G A, Bekins B A, Ge S. 2014. Sharp increase in central Oklahoma seismicity since 2008 induced by massive wastewater injection. Science, 345: 448–451

Kostrov B V. 1974. Seismic moment and energy of earthquakes, and seismic flow of rock. U.S.S.R. Academy of Sciences Izvestiya Phys Solid Earth, 1: 23–44

Kumazawa T, Ogata Y. 2014. Nonstationary ETAS models for nonstandard earthquakes. Ann Appl Stat, 8: 1825–1852

Kumazawa T, Ogata Y, Kimura K, Maeda K, Kobayashi A. 2016. Background rates of swarm earthquakes that are synchronized with volumetric strain changes. Earth Planet Sci Lett, 442: 51–60

Lei X, Ma S, Chen W, Pang C, Zeng J, Jiang B. 2013. A detailed view of the injection-induced seismicity in a natural gas reservoir in Zigong, southwestern Sichuan Basin, China. J Geophys Res-Solid Earth, 118: 4296–4311

Li Y G, Leary P, Aki K, Malin P. 1990. Seismic trapped modes in the Oroville and San Andreas fault zones. Science, 249: 763–766

Liu Y, Xu L, Yang D. 2011. Pore pressure diffusion characteristics of Longtan reservoir-induced-earthquake (in Chinese). Chin J Geophys, 54: 1028–1037, doi: 10.3969/j.issn.0001-5733.2011.04.017

Llenos A L, Michael A J. 2013. Modeling earthquake rate changes in Oklahoma and Arkansas: Possible signatures of induced seismicity. Bull Seismol Soc Am, 103: 2850–2861

Llenos A L, Michael A J. 2016. Characterizing potentially induced earthquake rate changes in the Brawley seismic zone, southern California. Bull Seismol Soc Am, 106: 2045–2062

Massonnet D, Holzer T, Vadon H. 1997. Land subsidence caused by the East Mesa Geothermal Field, California, observed using SAR interferometry. Geophys Res Lett, 24: 901–904

Massonnet D, Feigl K L. 1998. Radar interferometry and its application to changes in the Earth's surface. Rev Geophys, 36: 441–500

Michelet S, Toksöz M N. 2007. Fracture mapping in the Soultz-sous-Forêts geothermal field using microearthquake locations. J Geophys Res, 112: B07315

McGarr A. 2014. Maximum magnitude earthquakes induced by fluid injection. J Geophys Res-Solid Earth, 119: 1008–1019

McGarr A, Bekins B, Burkardt N, Dewey J, Earle P, Ellsworth W, Ge S, Hickman S, Holland A, Majer E, Rubinstein J, Sheehan A. 2015. Coping with earthquakes induced by fluid injection. Science, 347: 830–831

McGarr A, Simpson D, Seeber L. 2002. Case histories of induced and triggered seismicity. In: Lee W H K, Kanamori H, Jenning P C, Kisslinger C, eds. International Handbook of Earthquake and Engineering Seismology, Part A. 647–661

McNamara D E, Benz H M, Herrmann R B, Bergman E A, Earle P, Holland A, Baldwin R, Gassner A. 2015. Earthquake hypocenters and focal mechanisms in central Oklahoma reveal a complex system of reactivated subsurface strike-slip faulting. Geophys Res Lett, 42: 2742–2749

Nicholson C, Wesson R L. 1992. Triggered earthquakes and deep well activities. PAGEOPH, 139: 561–578

Ogata Y. 1988. Statistical models for earthquake occurrences and residual analysis for point processes. J Am Statistical Association, 83: 9–27

Ogata Y. 1998. Space-time point-process models for earthquake occurrences. Ann Institute Statistical Math, 50: 379–402

Ogata Y, Katsura K, Tanemura M. 2003. Modelling heterogeneous space-time occurrences of earthquakes and its residual analysis. Applied Statistics (JRSSC), 52(Part4): 499–509

Ogata Y, Zhuang J. 2006. Space–time ETAS models and an improved extension. Tectonophysics, 413: 13–23

Omori F. 1894. On the aftershocks of earthquakes. J College of Science, Imperial University of Tokyo, 7: 111–200

Petersen M D, Mueller C S, Moschetti M P, Hoover S M, Rubinstein J L, Llenos A L, Michael A J, Ellsworth W L, McGarr A F, Holland A A, Anderson J. G. 2015. Incorporating Induced Seismicity in the 2014 United States National Seismic Hazard Model—Results of the 2014 Workshop and Sensitivity Studies. USGS Open-File Report 2015–1070 (https://dx.doi.org/10.3133/ofr20151070)

Petersen M D, Mueller C S, Moschetti M P, Hoover S M, Llenos A L, Ellsworth W L, Michael A J, Rubinstein J L, McGarr A F, Rukstales K S. 2016. Seismic-hazard forecast for 2016 including induced and natural earthquakes in the central and eastern United States. Seismol Res Lett, 87: 1327–1341

Pollitz F F, Wicks C, Schoenball M, Ellsworth W, Murry M. 2017. Geodetic slip model of the 3 September 2016 M_w5.8 Pawnee, Oklahoma, earthquake: Evidence for fault-zone collapse. Seismol Res Lett, 88, doi: 10.1785/0220170002

Priolo E, Romanelli M, Plasencia Linares M P, Garbin M, Peruzza L, Romano M A, Marotta P, Bernardi P, Moratto L, Zuliani D, Fabris P. 2015. Seismic monitoring of an underground natural gas storage facility: The Collalto seismic network. Seismol Res Lett, 86: 109–123

Raleigh C B, Healy J H, Bredehoeft J D. 1976. An experiment in earthquake control at rangely, Colorado. Science, 191: 1230–1237

Rosen P A, Hensley S, Joughin I R, Li F K, Madsen S N, Rodriguez E, Goldstein R M. 2000. Synthetic aperture radar interferometry. Proc IEEE, 88: 333–382

Rudnicki J W. 1986. Fluid mass sources and point forces in linear elastic diffusive solids. Mech Mater, 5: 383–393

Samsonov S, Czarnogorska M, White D. 2015. Satellite interferometry for high-precision detection of ground deformation at a carbon dioxide storage site. Int J Greenhouse Gas Control, 42: 188–199

Segall P. 1989. Earthquakes triggered by fluid extraction. Geology, 17:

942–946

Segall P, Lu S. 2015. Injection-induced seismicity: Poroelastic and earthquake nucleation effects. J Geophys-Res Solid Earth, 120: 5082–5103

Schultz R, Stern V, Gu Y J. 2014. An investigation of seismicity clustered near the Cordel Field, west central Alberta, and its relation to a nearby disposal well. J Geophys-Res Solid Earth, 119: 3410–3423

Schultz R, Stern V, Novakovic M, Atkinson G, Gu Y J. 2015. Hydraulic fracturing and the Crooked Lake Sequences: Insights gleaned from regional seismic networks. Geophys Res Lett, 42: 2750–2758

Schultz R, Wang R, Gu Y J, Haug K, Atkinson G. 2017. A seismological overview of the induced earthquakes in the Duvernay play near Fox Creek, Alberta. J Geophys Res-Solid Earth, 122: 492–505

Shapiro S A, Dinske C. 2009. Scaling of seismicity induced by nonlinear fluid-rock interaction. J Geophys Res, 114: B09307

Shapiro S A, Dinske C, Kummerow J. 2007. Probability of a given-magnitude earthquake induced by a fluid injection. Geophys Res Lett, 34: L22314

Shapiro S A, Dinske C, Langenbruch C, Wenzel F. 2010. Seismogenic index and magnitude probability of earthquakes induced during reservoir fluid stimulations. Leading Edge, 29: 304–309

Shirzaei M, Ellsworth W L, Tiampo K F, González P J, Manga M. 2016. Surface uplift and time-dependent seismic hazard due to fluid injection in eastern Texas. Science, 353: 1416–1419

Skoumal R J, Brudzinski M R, Currie B S. 2015. Earthquakes induced by hydraulic fracturing in Poland Township, Ohio. Bull Seismol Soc Am, 105: 189–197

Steacy S, Gomberg J, Cocco M. 2005. Introduction to special section: Stress transfer, earthquake triggering, and time-dependent seismic hazard. J Geophys Res, 110: B05S01

Suckale J. 2009. Induced seismicity in hydrocarbon fields. Adv Geophys, 51: 55–106, doi: 10.1016/S0065-2687(09)05107-3

Sumy D F, Cochran E S, Keranen K M, Wei M, Abers G A. 2014. Observations of static Coulomb stress triggering of the November 2011 M 5.7 Oklahoma earthquake sequence. J Geophys Res-Solid Earth, 119: 1904–1923

Talwani P. 1997. On the nature of reservoir-induced seismicity. Pure appl geophys, 150: 473–492

Utsu T. 1970. Aftershock and earthquake statistics (ii): Further investigation of aftershocks and other earthquake sequences based on a new classication of earthquake sequences. J Faculty Sci Hokkaido Univ Ser VII Geophys, 3: 197–266

van der Elst N J, Page M T, Weiser D A, Goebel T H W, Hosseini S M. 2016. Induced earthquake magnitudes are as large as (statistically) expected. J Geophys Res-Solid Earth, 121: 4575–4590

Walsh F R, Zoback M D. 2016. Probabilistic assessment of potential fault slip related to injection-induced earthquakes: Application to north-central Oklahoma, USA. Geology, 44: 991–994

Wang B, Ge H, Yang W, Wang W, Wang B, Wu G, Su Y. 2012. Transmitting seismic station monitors fault zone at depth. Eos Trans Am Geophys Union, 93: 49–50

Wang B, Harrington R M, Liu Y, Yu H, Carey A, van der Elst N J. 2015. Isolated cases of remote dynamic triggering in Canada detected using cataloged earthquakes combined with a matched-filter approach. Geophys Res Lett, 42: 5187–5196

Wang D, Li Y, Nie Z, Wang T, Qiao X, Li J, Yu P, Cheng R. 2016. Study on the cap rock deformation of Hutubi underground gas storage by GPS. Earthq Res China, 32: 397–406

Wang P, Small M J, Harbert W, Pozzi M. 2016. A bayesian approach for assessing seismic transitions associated with wastewater injections. Bull Seismological Soc Am, 106: 832–845

Wang R, Gu Y J, Schultz R, Zhang M, Kim A. 2017. Source characteristics and geological implications of the January 2016 induced earthquake swarm near Crooked Lake, Alberta. Geophys J Int, doi: 10.1093/gji/g9x204

Weingarten M, Ge S, Godt J W, Bekins B A, Rubinstein J L. 2015. High-rate injection is associated with the increase in U.S. mid-continent seismicity. Science, 348: 1336–1340

Weng H, Yang H, Zhang Z, Chen X. 2016. Earthquake rupture extents and coseismic slips promoted by damaged fault zones. J Geophys Res-Solid Earth, 121: 4446–4457

Wibberley C A J, Yielding G, Di Toro G. 2008. Recent advances in the understanding of fault zone internal structure: A review. Geol Soc London Spec Publ, 299: 5–33

Wong I, Nemser E, Bott J, Dober M. 2015. White Paper Induced Seismicity and Traffic Light Systems as Related to Hydraulic Fracturing in Ohio. Ohio Oil and Gas Association (http://www.ooga.org/resource/resmgr/Files/OOGA_IS_TLS_White_Paper_fina.pdf)

Yang H, Zhu L, Chu R. 2009. Fault-plane determination of the 18 April 2008 Mount Carmel, Illinois, earthquake by detecting and relocating aftershocks. Bull Seismol Soc Am, 99: 3413–3420

Yang H. 2010. Study of earthquake fault zone structures by aftershock location and high-frequency waveform modelling. Doctoral Dissertation. Saint Louis: Saint Louis University

Yang H. 2015. Recent advances in imaging crustal fault zones: A review. Earthq Sci, 28: 151–162

Yang H, Zhu L. 2010. Shallow low-velocity zone of the San Jacinto fault from local earthquake waveform modelling. Geophys J Int, 183: 421–432

Yang H, Zhu L, Cochran E S. 2011. Seismic structures of the Calico fault zone inferred from local earthquake travel time modelling. Geophys J Int, 186: 760–770

Yang H, Li Z, Peng Z, Ben-Zion Y, Vernon F. 2014. Low-velocity zones along the San Jacinto Fault, Southern California, from body waves recorded in dense linear arrays. J Geophys Res-Solid Earth, 119: 8976–8990

Yang H, Lin J, Yin J, Yao H. 2015. Tectonic settings of the 2015 M_w 8.3 Coquimbo, Chile earthquake and its implications on megathrust earthquakes (in Chinese). Chin Sci Bull, 60: 3549–3556, doi: 10.1360/N972015-01110

Yeck W L, Hayes G P, McNamara D E, Rubinstein J L, Barnhart W D, Earle P S, Benz H M. 2017. Oklahoma experiences largest earthquake during ongoing regional wastewater injection hazard mitigation efforts. Geophys Res Lett, 44: 711–717

Yin J X, Yang H F, Yao H J, Weng H H. 2016. Coseismic radiation and stress drop during the 2015 M_w 8.3 Illapel, Chile megathrust earthquake. Geophys Res Lett, 43: 1520–1528

Yin J X, Yao H J, Yang H F, Liu J, Qin W Z, Zhang H J. 2017. Frequency-dependent rupture process, stress change, and seismogenic mechanism of the 25 April 2015 Nepal Gorkha M_w 7.8 earthquake. Sci China Earth Sci, 60: 796–808

Yue H, Lay T. 2011. Inversion of high-rate (1 sps) GPS data for rupture process of the 11 March 2011 Tohoku earthquake (M_w 9.1). Geophys Res Lett, 38: L00G09

Zaliapin I, Ben-Zion Y. 2016. Discriminating characteristics of tectonic and human-induced seismicity. Bull Seismol Soc Am, 106: 846–859

Zhang B, Wang B, Yang H, Ji Z, Hou J, Li L. 2017. Seismicity around the Hutubi underground gas storage, Xinjiang, China. SEG Workshop on Microseismic Technologies and Applications, Hefei, China

Zhang H, Eaton D W, Li G, Liu Y, Harrington R M. 2016. Discriminating induced seismicity from natural earthquakes using moment tensors and source spectra. J Geophys Res-Solid Earth, 121: 972–993

Zoback M D, Gorelick S M. 2012. Earthquake triggering and large-scale geologic storage of carbon dioxide. Proc Natl Acad Sci USA, 109: 10164–10168

Zhuang J, Ogata Y, Vere-Jones D. 2002. Stochastic declustering of space-time earthquake occurrences. J Am Statistical Association, 97: 369–380

Zhuang J. 2011. Next-day earthquake forecasts for the Japan region generated by the ETAS model. Earth Planet Space, 63: 207–216